Materials Science and Technology

ISSN: 0267-0836 (Print) 1743-2847 (Online) Journal homepage: www.tandfonline.com/journals/ymst20

Kinetics of phase decomposition processes: numerical solutions to Cahn–Hilliard equation

M. I. M. Copetti & C. M. Elliott

To cite this article: M. I. M. Copetti & C. M. Elliott (1990) Kinetics of phase decomposition processes: numerical solutions to Cahn–Hilliard equation, Materials Science and Technology, 6:3, 273-284, DOI: 10.1179/mst.1990.6.3.273

To link to this article: https://doi.org/10.1179/mst.1990.6.3.273

Published online: 18 Jul 2013.

Kinetics of phase decomposition processes: numerical solutions to Cahn–Hilliard equation

Finite difference methods giving approximate solutions to the Cahn–Hilliard equation for phase separation in binary alloys and the results of numerical experiments in two dimensional space are described. Nucleation and growth and spinodal decomposition are considered. *MST/1199*

M. I. M. Copetti
C. M. Elliott

 The authors are in the School of Mathematical and Physical Sciences, University of Sussex, Brighton. Ms Copetti is a CAPES fellow from Departamento de Matemática e NEPAE, Universidade Federal de Santa Maria, Brazil.

Introduction

In this paper the numerical approximation of the Cahn–Hilliard model[1–3] for phase separation in binary alloys is considered. When a single phase homogeneous system composed of species A and B, at high temperature and in thermal equilibrium, is cooled rapidly to a uniform temperature below a critical temperature in the two phase coexistence region (Fig. 1), phase separation may occur. Depending on where the quench leaves the system, phase separation proceeds via nucleation or spinodal decomposition.

Below a critical temperature the coarse grained Ginzburg–Landau free energy ψ of the system has the double well shape shown in Fig. 2. The region where $\psi'' < 0$, (u_a^s, u_b^s), is called the spinodal and the two points u_a and u_b, where the supporting tangent touches the curve, are the binodal points. Here the local concentration (mole fraction) $u(\boldsymbol{x}, t)$ of species B, at point $\boldsymbol{x}$ and time t, is the relevant order parameter.[3]

Within the spinodal the system is unstable in the sense that infinitesimal fluctuations in composition about the average composition u_m of the system reduce the overall free energy and are sufficient to initiate spinodal decomposition. The system separates into two phases with respective concentrations u_a and u_b; this is the lower energy state. Within the metastable region small fluctuations increase the free energy, but a finite, sufficiently large perturbation may reduce the energy and cause phase separation. This phase separation is considered to proceed via nucleation and growth and the equilibrium state of the system consists again of two coexisting phases. Beyond the coexistence curve, to the left of u_a, and to the right of u_b, the system is stable and any perturbation is absorbed by the system. Thus, the only equilibrium state is the homogeneous single phase state.

Cahn–Hilliard equation

A possible mathematical continuum model for phase separation in binary alloys was proposed by Cahn and Hilliard.[1] The alloy occupies the spatial domain Ω. The time evolution of the concentration $u(\boldsymbol{x}, t)$, for $\boldsymbol{x} \in \Omega$ and $t > 0$, after the quench is described by the Cahn–Hilliard equation

$$\frac{\partial u}{\partial t} = M\nabla^2[\psi'(u) - \gamma\nabla^2 u] \quad \ldots\ldots\ldots \quad (1)$$

Here $M > 0$ is the mobility (assumed to be constant) and $\gamma > 0$ is a phenomenological constant modelling the effect of interfacial energy. The gradient operator is denoted by ∇ and the Laplacian operator by ∇^2.

For small t, i.e. the early stages of spinodal decomposition when the fluctuations in amplitude of the concentration are small, it is possible to consider the linear approximation about the average concentration u_m

$$\frac{\partial u}{\partial t} = M\psi''(u_m)\nabla^2(u - \gamma\nabla^2 u)$$

The solution of this equation is

$$u(\boldsymbol{x}, t) - u_m = \sum_{\mathbf{k}} \mathbf{A}_{\mathbf{k}} \exp(-R_{|\mathbf{k}|}t) \exp(\mathrm{i}\mathbf{k}\cdot\boldsymbol{x})$$

where $A_{\mathbf{k}}$ is amplitude and

$$R_{|\mathbf{k}|} = |\boldsymbol{k}|^2[M\psi''(u_m) + \gamma|\boldsymbol{k}|^2]$$

is the amplification factor which is positive for values of u_m in the metastable region and negative for values of u_m in the spinodal for

$$|\boldsymbol{k}|^2 < \frac{-M\psi''(u_m)}{\gamma} \stackrel{\text{def}}{=} k_c^2$$

Therefore, any wave component present initially in $u(\boldsymbol{x}, 0)$ will grow or shrink exponentially with time according to whether $R_{|\mathbf{k}|}$ is negative or positive. Since $-R_{|\mathbf{k}|}$ has a maximum at $k_{max} = (1/\sqrt{2})k_c$, the Fourier components with wavelength $\lambda = 2\pi/k_{max}$ will grow most rapidly leading to a pattern of superposed waves with approximately this λ. The dependence of the amplification factor on the wave number for a quench within the unstable region is shown in Fig. 3.

Because of the exponential growth this linearisation is not valid in the later stages of spinodal decomposition. The range of validity and the degree of accuracy of the linear theory have been discussed[2,3] and there has been much controversy regarding these points.[4,5]

A parameter of great importance, which can be obtained experimentally from observed scattered intensity, is the structure factor $S(\boldsymbol{k}, t)$ defined as

$$S(\boldsymbol{k}, t) = |\hat{u}(\boldsymbol{k}, t)|^2$$

where $\hat{u}(\boldsymbol{k}, t)$ is the Fourier transform of $u(\boldsymbol{x}, t)$. The

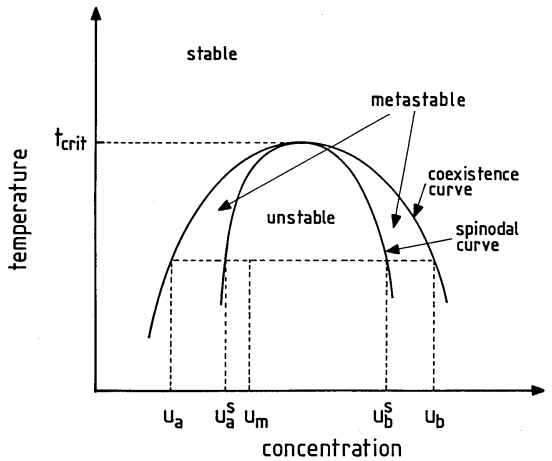

1 Phase diagram for binary alloy

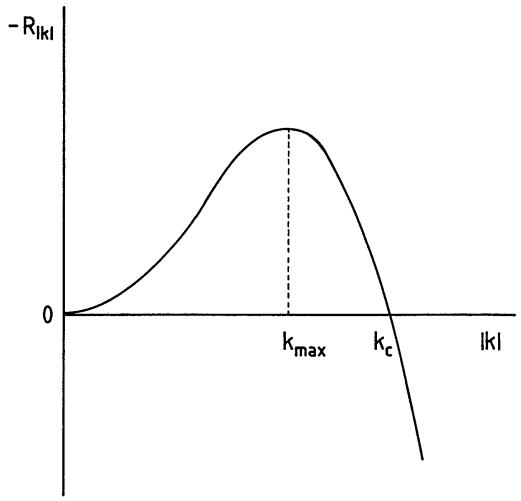

3 Amplification factor for quench within spinodal

linear theory of spinodal decomposition predicts an exponential growth in $S(\boldsymbol{k}, t)$ for $|k| < k_c$. Experimental evidence and numerical experiments on the nonlinear equation and discrete models (Ising type) suggest that, for large t, the value k_{max} where $S(\boldsymbol{k}, t)$ has its maximum behaves as $t^{-\alpha}$ with α ranging from 0·19 to 0·35;[3,6,7] k_{max} is proportional to $1/D$ where D is a measure of the domain size and characterises the coarsening of domains.

Equation (1) can be rewritten as

$$\frac{\partial u}{\partial t} = M\nabla^2 w \quad \ldots\ldots\ldots\ldots \quad (2a)$$

where

$$w = \phi(u) - \gamma\nabla^2 u \quad \ldots\ldots\ldots\ldots \quad (2b)$$

is a generalised chemical potential with $\phi(u) = \psi'(u)$; $\psi(u)$, an approximation of the free energy, is taken to be a quartic polynomial in the concentration with a double well as shown in Fig. 2. It should be noted that, without loss of generality, $\psi(u) = \frac{\alpha}{4}(u^2 - \beta^2)^2$ may be taken; this follows because, with $\psi(u)$ as a quartic polynomial as is shown in Fig. 2, the binodal points u_a and u_b satisfy

$$\psi'(u_a) = \psi'(u_b) = \frac{\psi(u_a) - \psi(u_b)}{u_a - u_b} \stackrel{\text{def}}{=} \mu$$

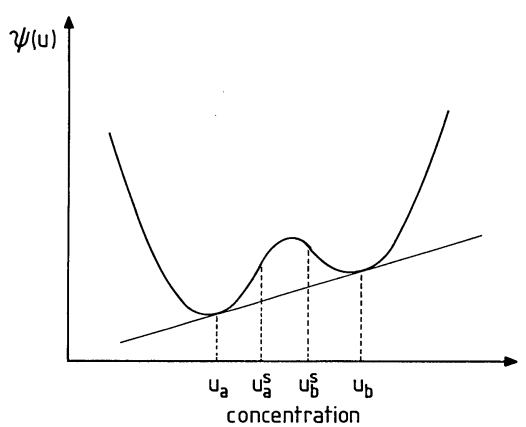

2 Free energy of system below critical temperature; (u_a^s, u_b^s) is spinodal interval and (u_a, u_a^s) ∪ (u_b^s, u_b) is metastable region

By setting

$$U = u - \frac{1}{2}(u_a + u_b)$$

and

$$\Psi(U) = [\psi(u) - \mu u] - [\psi(u_a) - \mu u_a]$$

so that

$$\Psi(U) = \frac{\alpha}{4}\left[U^2 - \frac{1}{4}(u_a - u_b)^2\right]^2$$

it is found that U solves

$$\frac{\partial U}{\partial t} = M\nabla^2[\Psi'(U) - \gamma\nabla^2 U]$$

For definiteness $\psi(u) = \frac{1}{4}(u^2 - 1)^2$ is taken, with binodal points $u_b = +1$ and $u_a = -1$ and spinodal interval $(-1/\sqrt{3}, 1/\sqrt{3})$. Equations (2*a*) and (2*b*) are supplemented by the initial condition

$$u(\boldsymbol{x}, 0) = u_0(\boldsymbol{x}) \quad \ldots\ldots\ldots\ldots \quad (2c)$$

and conditions on the boundary of Ω, where $\Omega \subset \boldsymbol{R}^q$, $q \leqslant 3$, is the region occupied by the system, are either Neumann conditions

$$\nabla w \cdot \boldsymbol{\eta} = \nabla u \cdot \boldsymbol{\eta} = 0 \quad \ldots\ldots\ldots\ldots \quad (2d)$$

where $\boldsymbol{\eta}$ is the unit normal vector to the boundary of Ω and ∇ denotes the gradient operator, or periodic boundary conditions.

Defining

$$\mathscr{F}(u) = \int_\Omega \left[\psi(u) + \frac{\gamma}{2}|\nabla u|^2\right] \mathrm{d}^q\boldsymbol{x}$$

gives

$$\frac{\mathrm{d}}{\mathrm{d}t}\mathscr{F}(u) + \int_\Omega |\nabla w|^2 \mathrm{d}^q\boldsymbol{x} = 0$$

and, in particular

$$\frac{\mathrm{d}}{\mathrm{d}t}\mathscr{F}(u) \leqslant 0$$

$\mathscr{F}(u)$ is the total energy being the sum of the free energy $\int_\Omega \psi(u)\mathrm{d}^q\boldsymbol{x}$ and the interfacial energy $\int_\Omega \frac{\gamma}{2}|\nabla u|^2\mathrm{d}^q\boldsymbol{x}$. The latter term measures interfacial energy because the inter-

face is associated with large gradients of the order parameter. The above calculation reveals that the Cahn–Hilliard equation for phase separation describes the evolution of an initial state into a lower energy state. There is also mass conservation as indicated by

$$\int_\Omega u(\boldsymbol{x}, t)\mathrm{d}^q\boldsymbol{x} = \int_\Omega u_0(\boldsymbol{x})\mathrm{d}^q\boldsymbol{x} = u_m|\Omega|$$

The existence of a solution to the problem described by equations (2*a*)–(2*d*) is proved in the paper by Elliott and Songmu.[8] Periodic boundary conditions are considered by Nicolaenko and Scheurer;[9] for a review of spinodal decomposition, *see* Gunton *et al.*[3] Mathematical aspects of the Cahn–Hilliard model are discussed by Elliott.[10]

The equilibrium solution of equations (2*a*)–(2*c*) solves the steady state problem

$$\phi(u) - \gamma\nabla^2 u = \sigma \quad (\boldsymbol{x} \in \Omega) \quad . \quad . \quad . \quad . \quad . \quad . \quad . \quad (3a)$$

$$\int_\Omega u(\boldsymbol{x})\mathrm{d}^q\boldsymbol{x} = \int_\Omega u_0(\boldsymbol{x})\mathrm{d}^q\boldsymbol{x} = u_m|\Omega| \quad . \quad . \quad . \quad . \quad (3b)$$

with either

$$\nabla u \cdot \boldsymbol{\eta} = 0 \quad (\text{on } \partial\Omega) \quad . \quad . \quad . \quad . \quad . \quad . \quad . \quad . \quad . \quad (3c)$$

or u periodic where the constant σ is determined by the mass conservation condition (equation (3*b*)).

A description of the steady state solutions for the problem described by equations (3*a*)–(3*c*) in one dimensional space is given by Novick-Cohen and Segel.[11] Carr *et al.*[12] focused their attention on the behaviour of solutions as $\gamma \to 0$. For numerical solutions to the time dependent Cahn–Hilliard equation in one dimensional space the reader is referred to Elliott and French.[13] For multi-dimensional space Modica[14] has shown that the limit of minimisers as $\gamma \to 0$ minimises the length of the interface between the two phases.

Numerical method

In this section, finite difference approximations of the Cahn–Hilliard equation

$$\frac{\partial u}{\partial t} = \nabla^2 w \quad (\boldsymbol{x} \in \Omega, t > 0) \quad . \quad . \quad . \quad . \quad . \quad . \quad (4a)$$

$$w = \phi(u) - \gamma\nabla^2 u \quad (\boldsymbol{x} \in \Omega, t > 0) \quad . \quad . \quad . \quad (4b)$$

$$u(\boldsymbol{x}, 0) = u_0(\boldsymbol{x}) \quad (\boldsymbol{x} \in \Omega) \quad . \quad . \quad . \quad . \quad . \quad . \quad . \quad . \quad (4c)$$

with periodic boundary conditions on the square $\Omega = [0, L] \times [0, L]$ are presented.

A uniform mesh of Ω with node points (x_i, y_j), $i, j = 0, 1, \ldots, N$, obtained by dividing the square Ω into N^2 squares with side $h = L/N$, is now considered. It is denoted by u_{ij}^n, $i, j = 0, 1, \ldots, N$, the value of u at point (x_i, y_j) and time t_n.

Let

$$\Delta^h u_{ij}^n = \frac{1}{h^2}\left(u_{i+1,j}^n + u_{i-1,j}^n - 4u_{ij}^n + u_{i,j+1}^n + u_{i,j-1}^n\right)$$

and

$$\partial_t u_{ij}^n = \frac{1}{k_n}\left(u_{ij}^n - u_{ij}^{n-1}\right)$$

where $k_n = t_n - t_{n-1}$ is the time step, be the approximations of $\nabla^2 u(x_i, y_j, t_n)$ and $\partial u/\partial t(x_i, y_j, t_n)$, respectively.

Then, the two finite difference approximations for the values of u at the mesh points (x_i, y_j), $i, j = 0, 1, \ldots, N-1$ are scheme (S1)

$$u_{ij}^{n+1} = u_{ij}^n - k_{n+1}\gamma\Delta^h(\Delta^h u_{ij}^n) + k_{n+1}\Delta^h\phi(u_{ij}^n)$$

and scheme (S2)

$$u_{ij}^{n+1} = u_{ij}^n - k_{n+1}\gamma\Delta^h(\Delta^h u_{ij}^{n+1}) + k_{n+1}\Delta^h\phi(u_{ij}^n)$$

respectively. Scheme (S1) is explicit and scheme (S2) is implicit in the fourth order term. Letting

$$u_{ij}^n = \sum_{r,s=0}^{N-1} a_{rs}^n \mathrm{E}_{rs}(i, j)$$

and

$$\Delta^h\phi(u_{ij}^n) = \sum_{r,s=0}^{N-1} b_{rs}^n \mathrm{E}_{rs}(i, j)$$

where

$$\mathrm{E}_{rs}(x, y) = \exp\left(\mathrm{i}\frac{2\pi}{N}xr\right)\exp\left(\mathrm{i}\frac{2\pi}{N}ys\right)$$

and noting that

$$\Delta^h u_{ij}^{n+1} = \sum_{r,s=0}^{N-1} a_{rs}^{n+1}\frac{\lambda_{rs}}{h^2}\mathrm{E}_{rs}(i, j)$$

with

$$\lambda_{rs} = -4 + 2\cos\left(\frac{2\pi r}{N}\right) + 2\cos\left(\frac{2\pi s}{N}\right)$$

the following is obtained, for scheme (S2)

$$\sum_{r,s=0}^{N-1}(a_{rs}^{n+1} - a_{rs}^n)\mathrm{E}_{rs}(i, j) = \left(-\frac{k_{n+1}\gamma}{h^4}\right) \times \sum_{r,s=0}^{N-1} a_{rs}^{n+1}\lambda_{rs}^2\mathrm{E}_{rs}(i, j) + k_{n+1}\sum_{r,s=0}^{N-1} b_{rs}^n\mathrm{E}_{rs}(i, j)$$

Thus

$$\left.\begin{aligned} a_{rs}^{n+1}\left(1 + \frac{k_{n+1}\gamma}{h^4}\lambda_{rs}^2\right) &= a_{rs}^n + k_{n+1}b_{rs}^n \\ (r, s &= 0, 1, \ldots, N-1)\end{aligned}\right\} \quad (5)$$

Using equation (5) and a fast Fourier transformation (FFT) to compute a_{rs}^n, b_{rs}^n, and u_{ij}^{n+1}, the approximate solution using scheme (S2) is obtained. *See* French and Nicolaides[15] for numerical computations on a Cahn–Hilliard model of solidification using a finite difference scheme and FFT. Numerical simulations in two dimensions have been carried out also by Rogers *et al.*[6] and Oono and Puri.[16]

Energy methods can be used to obtain[17] the stability conditions

$$k_{n+1} < \frac{h^4}{32\gamma + 8h^2\|g'(\xi_{n+1})\|_\infty} \quad n = 0, 1, \ldots$$

for scheme (S1) and

$$k_{n+1} < \frac{h^2}{8\|g'(\xi_{n+1})\|_\infty} \quad n = 0, 1, \ldots$$

for scheme (S2), where $g(u) = u^3$ and ξ_{n+1} depends on $\boldsymbol{u}^{n+1}$ and $\boldsymbol{u}^n$. With these conditions it results that $\mathscr{F}^h$, defined as

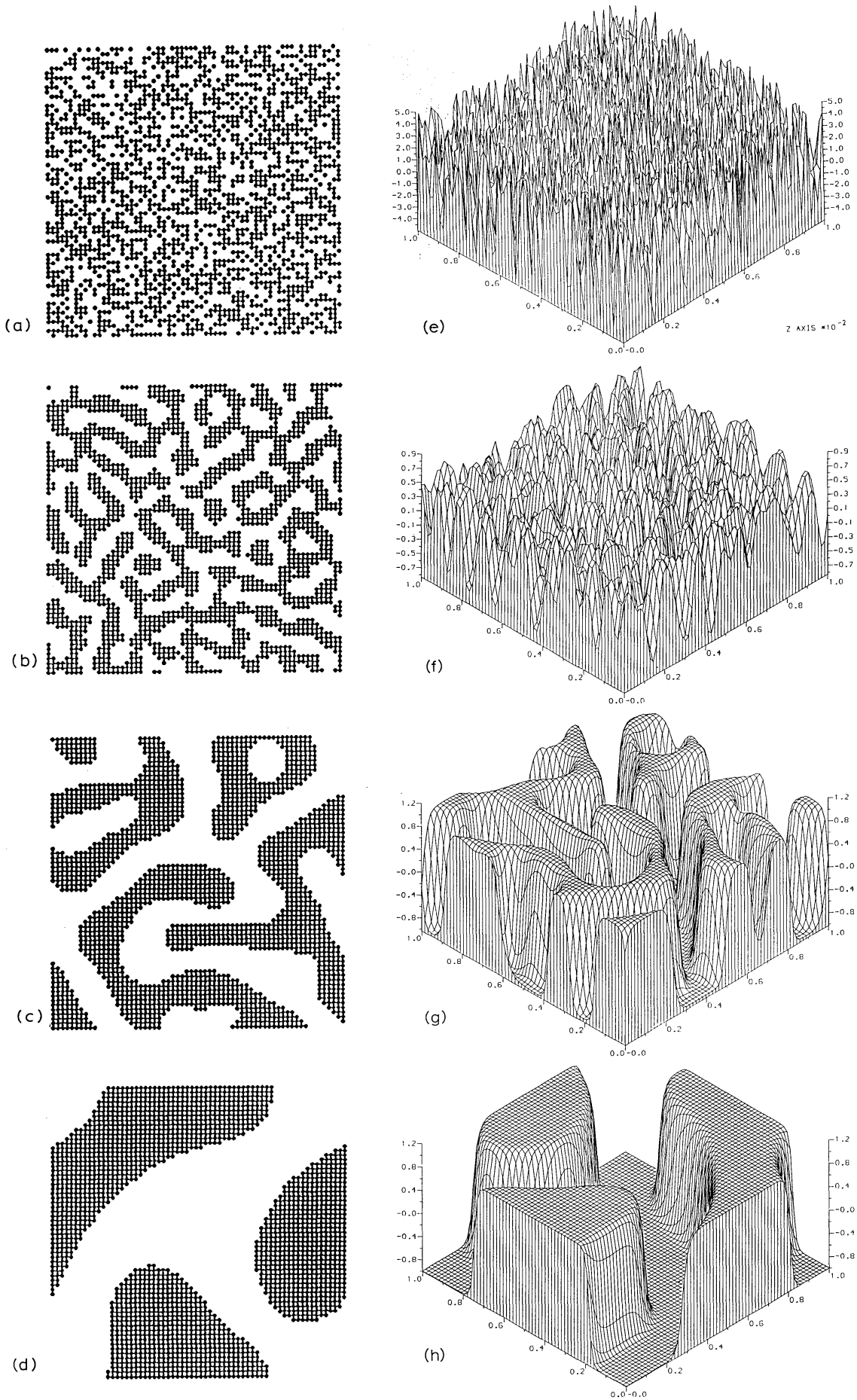

a, *e* $t = 0$; *b*, *f* $t = 10$; *c*, *g* $t = 200$; *d*, *h* $t = 3000$

4 Long time evolution patterns with $\gamma = 0{\cdot}5$; initial condition is random perturbation of homogeneous state $u = 0$; in *a–d* black dots correspond to $u > 0$ and in *e–h* concentration is plotted against (x, y); this applies throughout

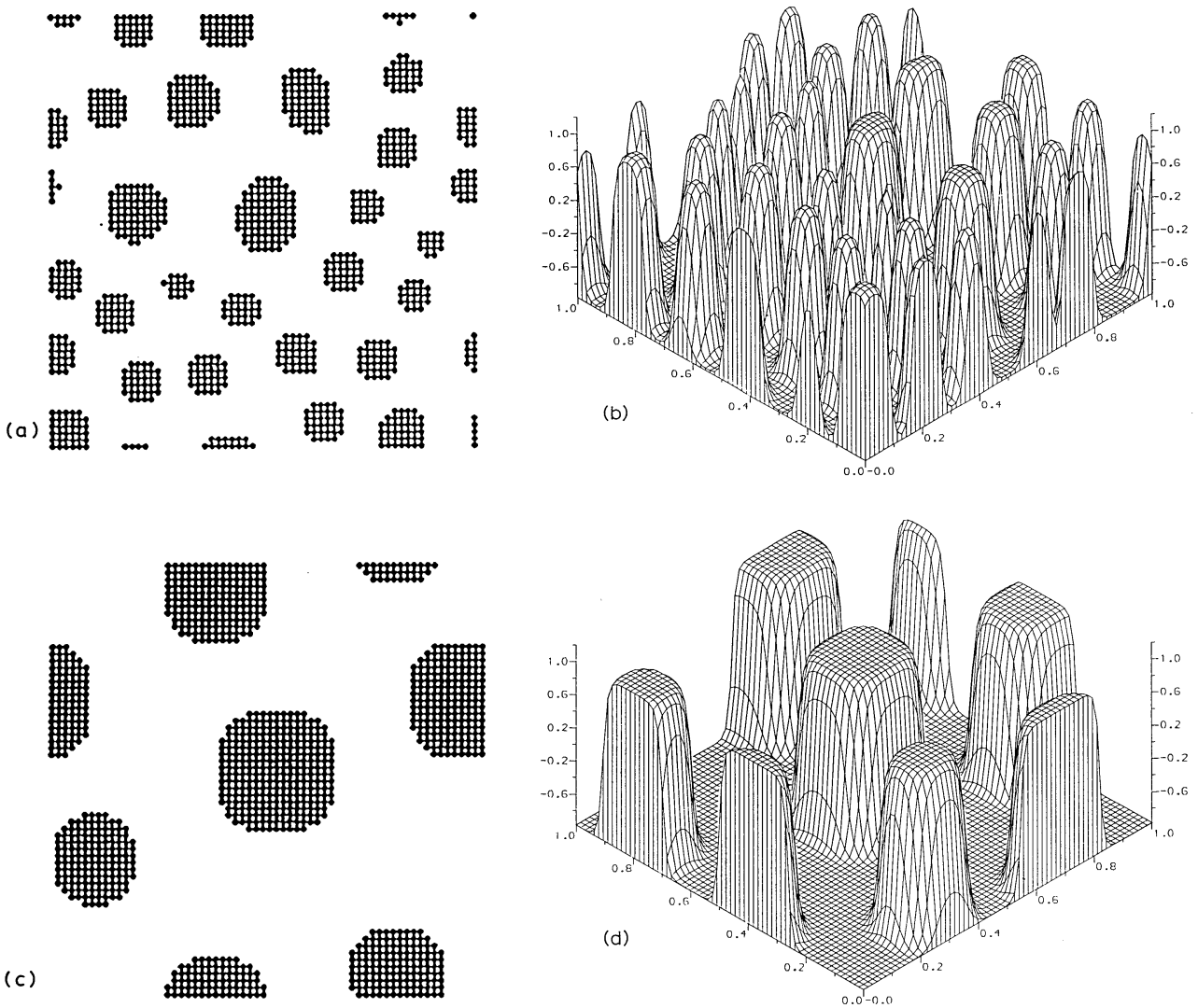

a, *b* $t = 200$; *c*, *d* $t = 3000$

5 Time evolution pattern of local concentration u from small perturbation (equation (6)) of state $u = u_m = -0{\cdot}45$, with $\gamma = 0{\cdot}5$

$$\mathscr{F}^h(\boldsymbol{u}^n) = h^2 \sum_{i,j=0}^{N-1} \psi(u_{ij}^n) + \frac{\gamma}{2} \sum_{i,j=0}^{N-1} u_{ij}^n(-u_{i+1,j}^n - u_{i-1,j}^n + 4u_{ij}^n - u_{i,j+1}^n - u_{i,j-1}^n)$$

satisfies, for schemes (S1) and (S2)

$$\frac{1}{k_{n+1}}[\mathscr{F}^h(\boldsymbol{u}^{n+1}) - \mathscr{F}^h(\boldsymbol{u}^n)] \leqslant 0$$

analogous to the decreasing energy property of the continuous problem.

Using the discrete Green's operator to approximate the inverse of the Laplacian operator with Neumann boundary conditions, it is possible to obtain[17] the stability condition for scheme (S2), independent of h

$$k_{n+1} < \frac{2\gamma}{\|g'(\xi_{n+1})\|_\infty^2} \quad n = 0, 1, \ldots$$

An *a priori* bound on the numerical solution of schemes (S1) and (S2) is not known. However, its maximum and minimum are expected to be close to +1 and −1, respectively. Since the number of operations required to calculate $\boldsymbol{u}^{n+1}$ is

$O(N^2)$

for scheme (S1) and

$O[N^2(\log_2 N)]$

for scheme (S2), and since the semi-implicit scheme (S2) allows a larger time step, scheme (S2) should be more efficient.

Numerical simulations

In this section some results of the simulations on the equation set (4*a*)–(4*c*) using the numerical approximation scheme (S2) are shown. A 64 × 64 ($N = 64$) mesh has been used on the square [0,64] × [0,64]. The simulations show that initial compositions which are perturbations of a uniform state in the spinodal interval evolve rapidly into a phase separated structure. After this rapid evolution a slow coarsening process takes place involving an increase of the size of the phase domains and a sharpening of the interfaces.

The time evolution of $u(\boldsymbol{x}, t)$ from initial condition

$$u_0(\boldsymbol{x}) = u_m + \xi(\boldsymbol{x}) \quad \ldots\ldots\ldots\ldots \quad (6)$$

where $\xi(\boldsymbol{x})$ is a random perturbation of the state $u = 0$ with values distributed uniformly between +0·05 and −0·05, is shown in Figs. 4 and 5 for mean values $u_m = 0$ and −0·45,

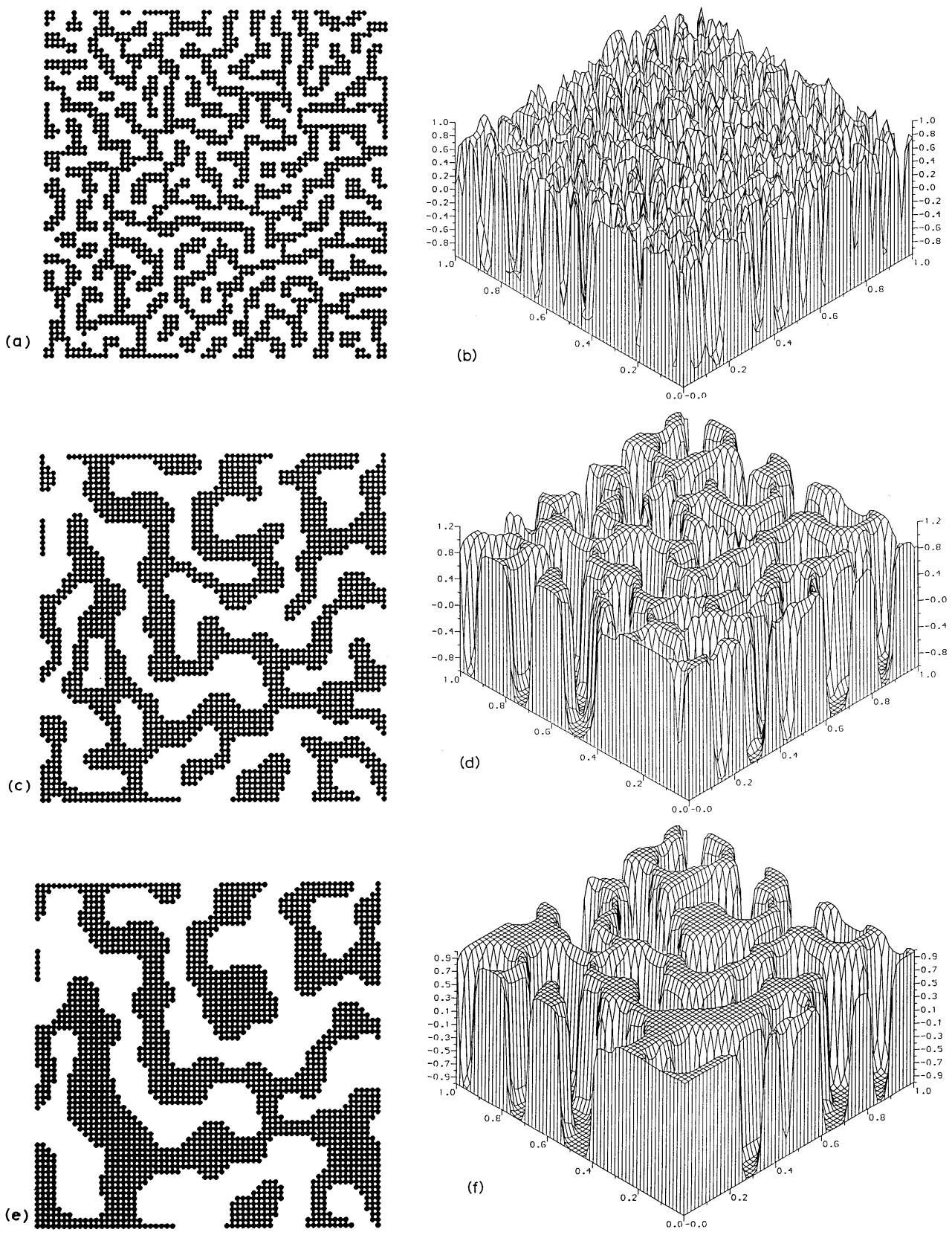

a, *b* $t = 10$; *c*, *d* $t = 200$; *e*, *f* $t = 3000$

6 Long time evolution from initial condition described in Fig. 4 with $\gamma = 0{\cdot}2$

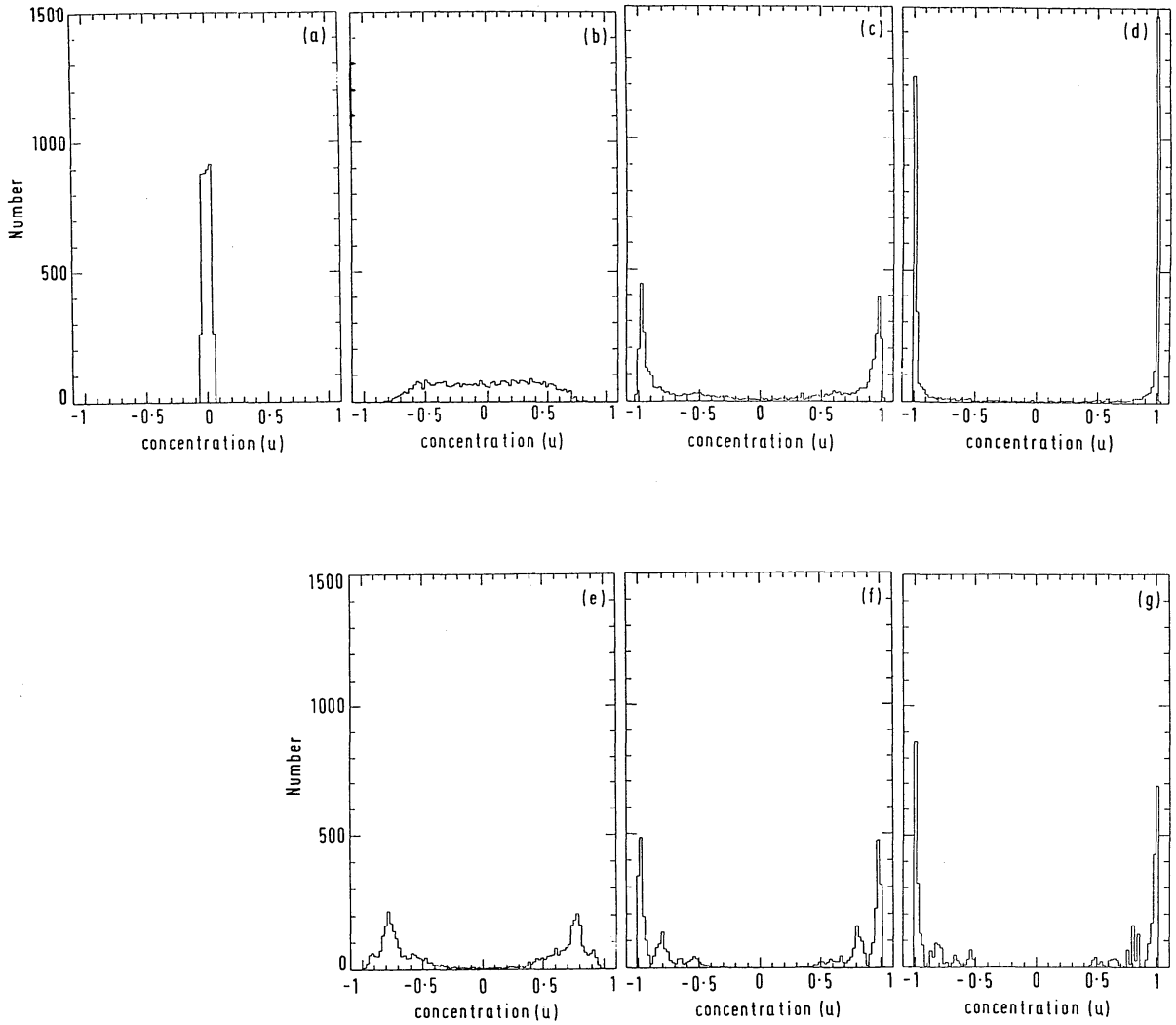

a $t = 0$; *b*, *e* $t = 10$; *c*, *f* $t = 200$; *d*, *g* $t = 3000$

7 Histograms of concentration for simulation of spinodal decomposition with $u_m = 0$ and *a–d* $\gamma = 0{\cdot}5$, *e–g* $\gamma = 0{\cdot}2$

respectively, in the spinodal region. Values of $\gamma = 0{\cdot}5$ and time step 0·1 were taken. In Figs. 4*a–d* the black dots denote phase B ($u > 0$) and in Figs. 4*e–h* the concentration is plotted against (x, y).

The evolution patterns for off critical quenches ($u_m \neq 0$) show circular domains appearing in the early stages of spinodal decomposition which contrast with the lamellar morphology of domains for mean value $u_m = 0$.

Computations were also carried out for values of $\gamma = 1$ and 0·2 with mean value $u_m = 0$; the results for $\gamma = 0{\cdot}2$ are shown in Fig. 6. In the early stages of spinodal decomposition, an increase in the number of interfaces has been observed when γ decreases in accordance with the linear theory which predicts a shorter wavelength for the waves that grow most rapidly. The interfaces also become steeper.

Histograms of concentration for simulation of spinodal decomposition have been plotted with $u_m = 0$ and $\gamma = 0{\cdot}5$ and 0·2 in Figs. 7*a–d* and 7*e–g*, respectively. The horizontal axis is divided into 100 subintervals and the vertical axis represents the number of mesh points the concentration values of which lie in the appropriate subinterval. The distribution of concentration becomes peaked around +1 and −1 and the interfaces sharpen with time. For $\gamma = 0{\cdot}2$, at $t = 3000$, there are virtually no values of u close to zero.

The time evolution of the structure factor

$$S(\boldsymbol{k}, t_n) = \frac{1}{N^2}\left|\sum_{j,l=0}^{N-1}(u_{jl}^n - u_m)\exp\left[-\frac{2\pi i}{N}(k_1 j + k_2 l)\right]\right|^2$$

and the autocorrelation function

$$G(\boldsymbol{r}, t_n) = \frac{1}{N^2}\sum_{j,l=0}^{N-1}(u_{jl}^n - u_m)(u_{j+r_1,l+r_2}^n - u_m)$$

$$= \frac{1}{N^2}\sum_{k_1,k_2=-N/2}^{N/2-1} S(\boldsymbol{k}, t_n)\exp\left[\frac{2\pi i}{N}(r_1 k_1 + r_2 k_2)\right]$$

where $\boldsymbol{k} = (k_1, k_2)$ and $\boldsymbol{r} = (r_1, r_2)$, with $r_1, r_2 = -\frac{N}{2}, \ldots, \frac{N}{2} - 1$, for the critical quench with $\gamma = 0{\cdot}5$ are shown in Figs. 8 and 9, respectively. It should be noted that $S(\boldsymbol{k}, t)$ and $G(\boldsymbol{r}, t)$ are periodic functions and that $S(\boldsymbol{O}, t) = 0$ owing to mass conservation.

Figure 8 shows a grey scale intensity of $S(\boldsymbol{k}, t)$ plotted against $\boldsymbol{k}/N$. In each square darker areas represent smaller values of $S(\boldsymbol{k}, t)$; however, the scales are not the same in each square. In the initial stages of spinodal decomposition, the formation of a brighter ring has been observed which collapses as the system evolves indicating the coarsening of domains. The radius of the ring at $t = 10$ is approximately $1/2\pi$ which accords with the value k_{max} given by the linear

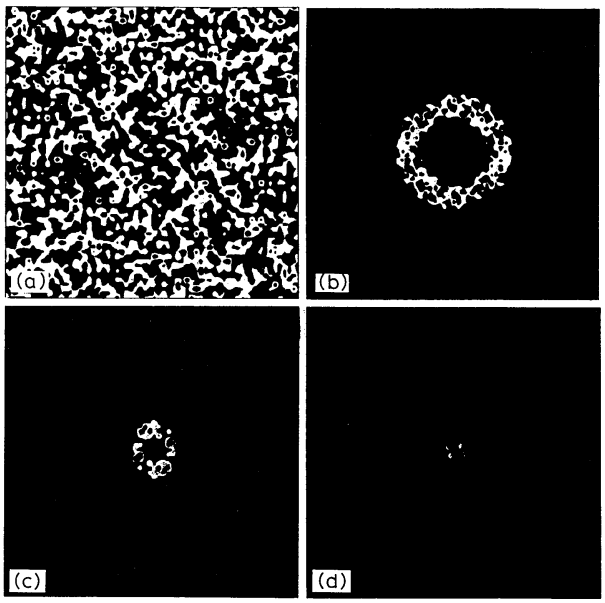

a $t = 0$; *b* $t = 10$; *c* $t = 200$; *d* $t = 3000$

8 Grey scale intensity of $S(k, t)$ for simulations shown in Fig. 4; darker areas represent smaller values of $S(k, t)$

theory. A similar phenomenon has been observed in scattering experiments carried out to investigate spinodal decomposition in binary fluids.[3]

For a critical quench with $\gamma = 0{\cdot}5$ long time computations were carried out until time $t = 63\,000$. At this time the pattern is a circle; therefore, the simulation was terminated because the system already had this configuration at $t = 36\,000$ and did not change. The results are shown in Fig. 10; the circular configuration can be readily seen by considering the periodic extension of the concentration to all of the plane.

To simulate phase separation of a system that is quenched in the metastable region an initial condition u_0 with nucleation centres was required. Thus, a small random perturbation u_0 of the homogeneous state $u = u_m = -0{\cdot}7$ was initiated with randomly placed nucleation centres with composition 0·98. Then, u_0 was modified at the nodes where $u_0 < 0$ to obtain an average composition of $-0{\cdot}7$. The results taking $\gamma = 0{\cdot}5$ are shown in Fig. 11.

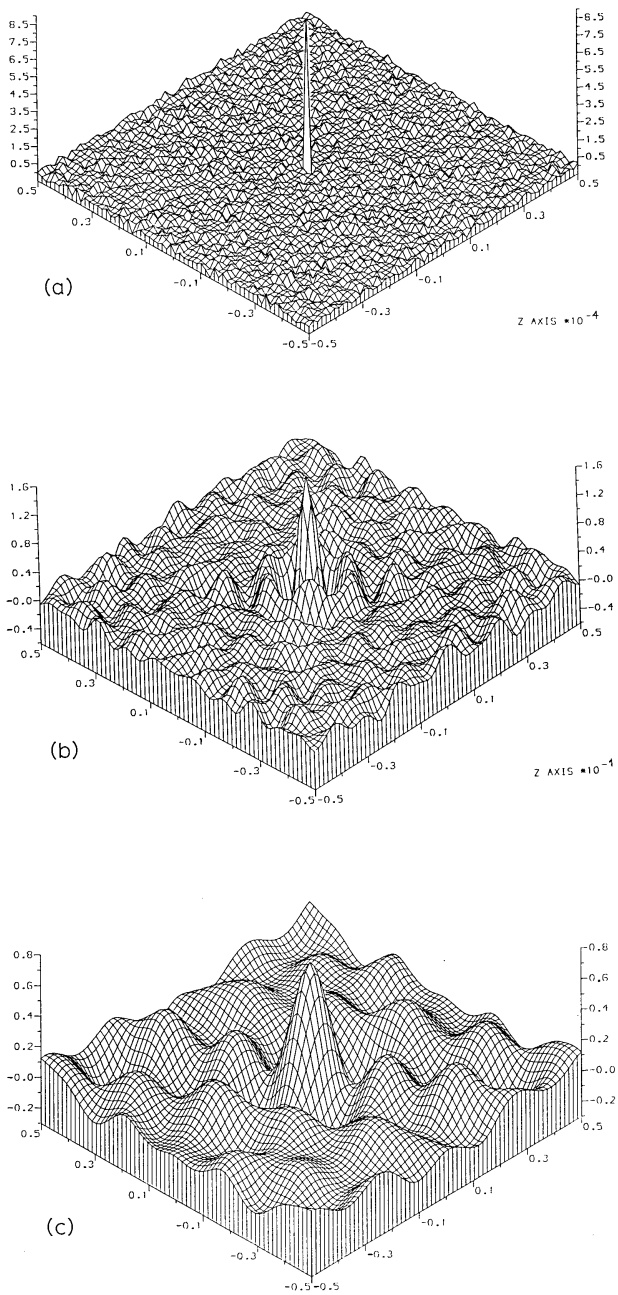

Conclusions

Numerical simulations in a two dimensional system with periodic boundary conditions of the Cahn–Hilliard model for phase separation in a binary alloy have been carried out using a semi-implicit finite difference scheme.

Dropletlike and interconnected domains are observed by simulating the quench of the system to different regions within the coexistence region. Histograms of concentration provided some insight into the evolution of the system and the morphology of the interfaces as γ changes. Some of the results are consistent with the conventional linear theory. It is noteworthy that these numerical simulations based on a differential equation model show striking qualitative agreement with experimental observations, some of which are discussed in other papers in this issue.

In future work results on the growth of domains are expected to be obtained using the averaged structure factor and the autocorrelation function.

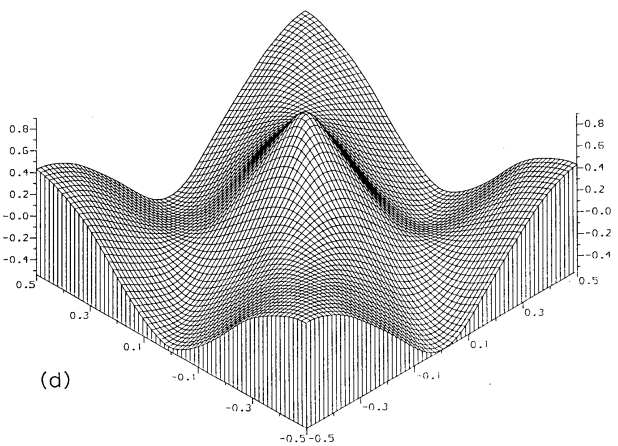

a $t = 0$; *b* $t = 10$; *c* $t = 200$; *d* $t = 3000$

9 Time evolution of autocorrelation function for simulations shown in Fig. 4 plotted against $1/N(r_1, r_2)$

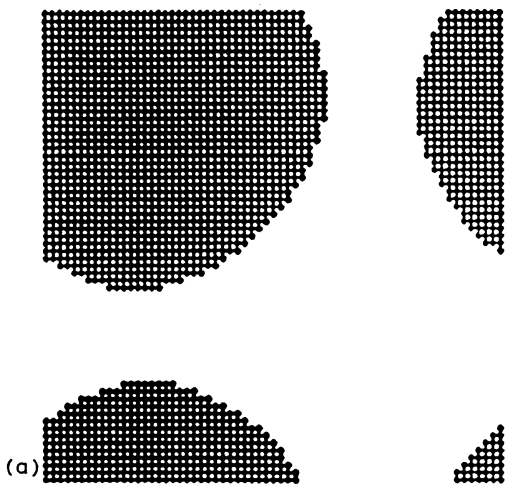

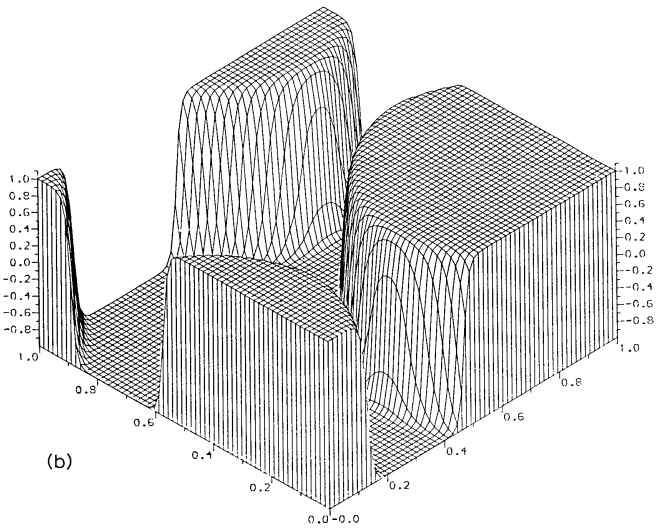

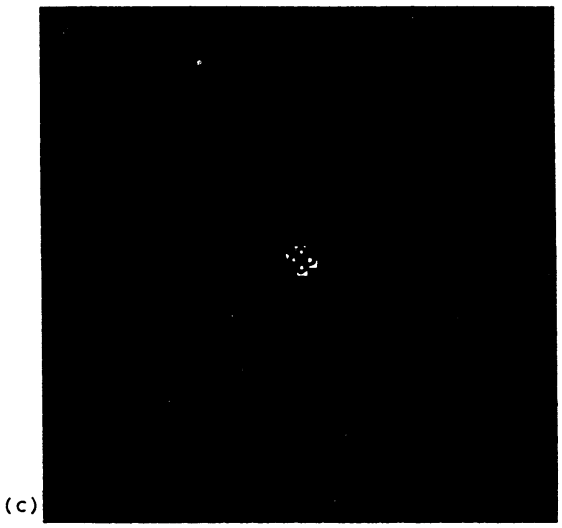

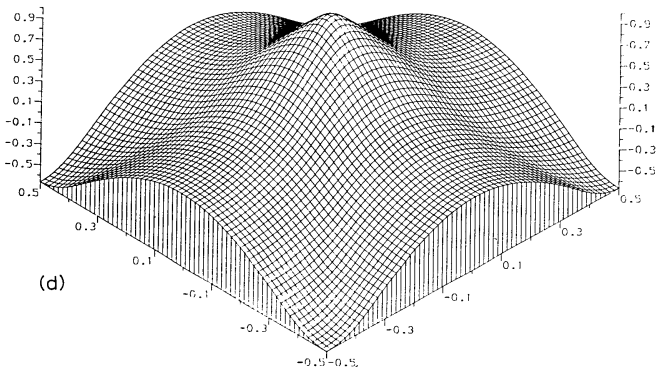

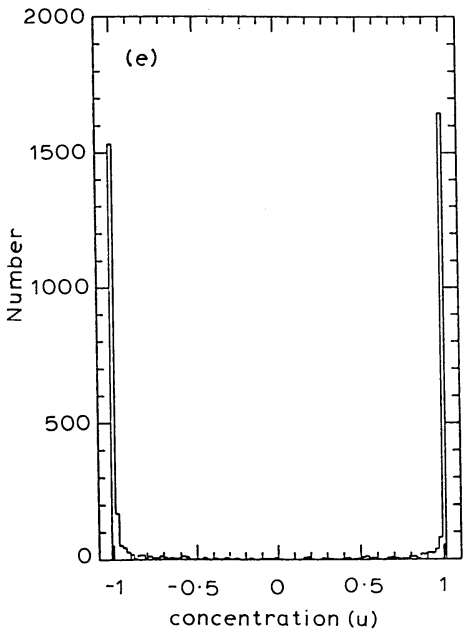

a, *b* evolution pattern with $u_m = 0$; *c* intensity of structure factor; *d* autocorrelation function; *e* histogram of concentration

10 Critical quench with $\gamma = 0{\cdot}5$ at $t = 63\,000$

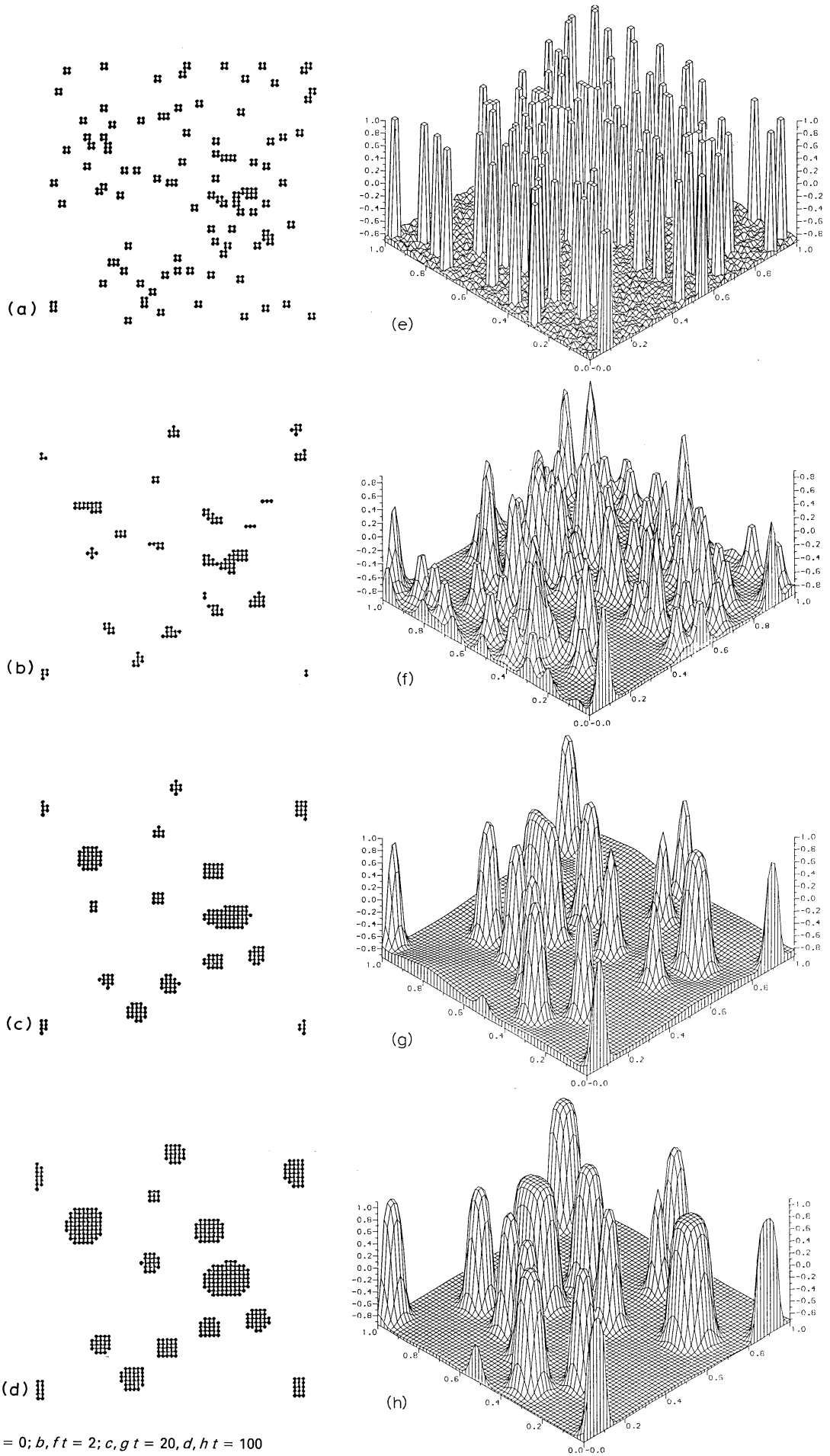

a, *e* $t = 0$; *b*, *f* $t = 2$; *c*, *g* $t = 20$, *d*, *h* $t = 100$

11 Evolution patterns for phase separation via nucleation and growth with $u_m = -0{\cdot}7$ and $\gamma = 0{\cdot}5$

Acknowledgments

The authors are grateful to Dr M. G. Hetherington for helpful conversations and suggestions. One of the authors (MIMC) would like to thank Dr M. Copetti and Mr J. Blowey for their assistance. This work was partially supported by the Brazilian institution CAPES.

References

1. J. W. CAHN and J. E. HILLIARD: *J. Chem. Phys*, 1958, **1**, 258–267.
2. J. S. LANGER, M. BAR-ON, and H. D. MILLER: *Phys. Rev. A*, 1975, **11**, (4), 1417–1429.
3. J. D. GUNTON, M. SAN-MIGUEL, and P. S. SAHNI: in 'Phase transitions and critical phenomena', (ed. C. Domb and J. L. Lebowitz), Vol. 8, 267–466; 1983, New York, Academic Press.
4. A. MILCHEV, D. W. HEERMANN, and K. BINDER: *Acta Metall.*, 1988, **36**, (2), 377–383.
5. K. R. ELDER, T. M. ROGERS, and R. C. DESAI: *Phys. Rev. B*, 1988, **38**, (7), 4725–4739.
6. T. M. ROGERS, K. R. ELDER, and R. C. DESAI: *Phys. Rev. B*, 1988, **37**, (16), 9638–9649.
7. J. L. LEBOWITZ, J. MARRO, and M. H. KALOS: *Acta Metall.*, 1982, **30**, 297–310.
8. C. M. ELLIOTT and Z. SONGMU: *Arch. Rat. Mech. Anal.*, 1986, **96**, (4), 339–357.
9. B. NICOLAENKO and B. SCHEURER: in 'Trends and practice of nonlinear analysis', (ed. A. Lakshimikantham); 1985, Amsterdam, North Holland.
10. C. M. ELLIOTT: in 'Mathematical models for phase change problems', (ed. J. Rodrigues), Int. Ser. Numerical Mathematics Vol. 88, 35–74; 1989, Stuttgart, FRG, Birkhäuser Verlag.
11. A. NOVICK-COHEN and L. SEGEL: *Physica*, 1984, **10D**, 277–298.
12. J. CARR, M. E. GURTIN, and M. SLEMROD: *Arch. Rat. Mech. Anal.*, 1984, **86**, 317–351.
13. C. M. ELLIOTT and D. A. FRENCH: *IMA J. Appl. Math.*, 1987, **38**, 97–128.
14. L. MODICA: *Arch. Rat. Mech. Anal.*, 1987, **98**, 123–142.
15. D. A. FRENCH and R. A. NICOLAIDES: *Appl. Num. Math.*, 1989, in press.
16. Y. OONO and S. PURI: *Phys. Rev. A*, 1988, **38**, (1), 434–453.
17. M. I. M. COPETTI: Thesis in preparation.